Hysteresis in kinking nonlinear elastic solids and the Preisach-Mayergoyz model

A. G. Zhou (周爱国),[1,*] S. Basu,[1] G. Friedman,[2] P. Finkel,[1,†] O. Yeheskel,[1,‡] and M. W. Barsoum[1]
[1]*Department of Materials Science and Engineering, Drexel University, Philadelphia, Pennsylvania 19104, USA*
[2]*Department of Electrical and Computer Engineering, Drexel University, Philadelphia, Pennsylvania 19104, USA*
(Received 14 April 2010; published 13 September 2010)

Herein we show that the stress-induced, dislocation-based, elastic hysteric loops of kinking nonlinear elastic solids—polycrystalline cobalt, 10 vol % porous Ti_2AlC, and fully dense Ti_3SiC_2—obey the scalar Preisach-Mayergoyz phenomenological model because they exhibit wiping out and congruency, two necessary and sufficient tenets of the model. We also demonstrate the power of the model in predicting the response of these materials to complex stress histories, as well as, determining the distributions of the threshold and friction stresses associated with the incipient kink bands—the fundamental microscopic units responsible for kinking nonlinear elasticity.

DOI: 10.1103/PhysRevB.82.094105 PACS number(s): 62.20.−x, 02.90.+p

I. INTRODUCTION

Mechanical hysteresis is common in solids. Granular solids, such as rocks, exhibit hysteresis that has been related to the internal friction of cracks that are common in such solids.[1–3] One of the hallmarks of this mechanism is a reduction in modulus with cycling.[4–6] This paper does not deal with this type hysteresis. As shown below, the hysteresis described herein is due to the reversible motion of dislocations; intergranular friction does not play a role. Probably the most convincing evidence for this state of affairs are the following facts: (i) at a given stress, fine-grained samples, with their much higher number of intergranular contacts dissipate less energy than their coarse-grained counterparts;[7–9] (ii) no cyclic softening is observed even after 100 cycles at 700 MPa in fine-grained Ti_3SiC_2.[10] Instead, after deformation at higher temperatures, cyclic hardening is observed.[7,10] (iii) Mg and Co—clearly not granular solids—were shown to follow the same relationships as Ti_3SiC_2. The remainder of this paper will thus focus on kinking and how it relates to hysteresis.

Recently we classified a large class of solids as kinking nonlinear elastic, KNE, for which the only requirement for belonging is plastic anisotropy.[7–9] This class is quite large and includes layered solids such as mica,[11] MAX phases,[7–9,12] and their solid solutions[13] as well as hexagonal solids such as graphite,[14] titanium,[15] magnesium,[16] cobalt,[17] sapphire,[18] and $LiNbO_3$,[19] among many others. When loaded, KNE solids outline fully reversible, reproducible, stress-strain hysteretic loops. This response has been attributed to the formation of dislocation-based incipient kink bands (IKBs)[7,8] comprised of multiple parallel dislocation loops in which dislocation segments, on either side, are of opposite signs. As shown by Frank and Stroh,[20] the shape of the IKBs endows them with, first, a threshold stress needed to nucleate them and, second, a driving force that results in their shrinkage, or elimination, when the load is reduced below a certain threshold.

Initially, our motivation was to try to obtain an appropriate model that described hysteresis and end-point memory of KNE solids. Following the lead of the geologists,[21–23] we tested the Preisach model. First developed to describe ferromagnetic hysteresis,[24,25] the Preisach model is based on the idea that macroscopically observed irreversible processes can be decomposed into *independent* switching events described by *independent* bistable relays. Mayergoyz,[26,27] recognizing that the Preisach model offered a general mathematical framework for the description of hysteresis of different physical origins, derived the necessary and sufficient conditions for representation of any given hysteresis by the Preisach model. These conditions are: first, that each local stress maximum wipes out the effect of other local stress maxima below it, and second, congruency of the hysteresis loops obtained via cycles with the same end points of input, but different prehistories. Mayergoyz called these properties wiping out and congruency, respectively. Thereafter the Preisach model was renamed the Preisach-Mayergoyz, or PM, model.

Before the PM model can be used it is essential to establish that wiping out and congruency are indeed valid. It should be noted that Guyer *et al.*[21,28] and Ortín[29] successfully applied this model to describe the nonlinear elastic response of granular geological materials and a shape memory alloy, respectively. And while previous work has clearly shown wiping out, as far as we are aware, dislocation-based congruency has *never* been reported in mechanical systems. In this paper, we present the experimental evidence that verifies that the PM model can indeed be used to describe the response of KNE solids to stress, σ, and consequently illustrate the predictive power of this conclusion. Most importantly, we show that the model can be used to calculate the *distributions* of the onset and friction stresses associated with the IKBs—the fundamental microscopic units responsible for kinking nonlinear elasticity. Before presenting the experimental evidence it is important to summarize our KNE model and how it relates to the PM model and to briefly explain kink band formation.

Kink bands have been invoked to explain the deformation of numerous materials and structures including organic crystals,[30] card decks,[31] rubber laminates,[32] oriented polymer fibers,[32–36] wood,[37] graphite fibers,[38,39] laminated C-C and C-epoxy composites,[40–42] among others.

However, outside geology,[43–45] the formation of kink bands in crystalline solids, has been for the past 70 years, and since first reported by Orowan,[46] more of an afterthought. Orowan induced kink band formation when he com-

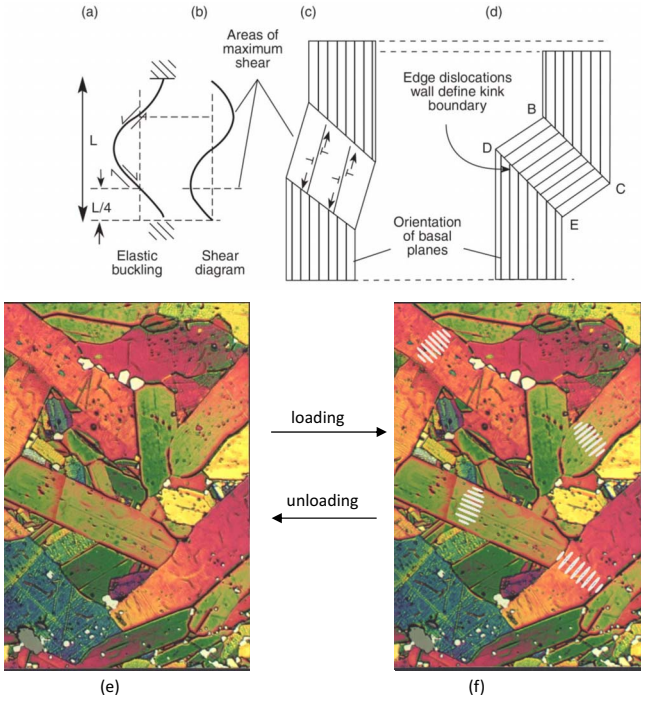

FIG. 1. (Color online) Schematic of kink band formation: [(a)–(d)] after Hess and Barrett (Ref. 47) (a) elastic buckling, (b) corresponding shear diagram, (c) initiation of pairs of dislocations in areas of maximum shear. (d) Kink band and kink boundaries comprised of edge dislocations of one sign giving rise to the signature stove-pipe configuration; (e) schematic of microstructure under no load (f) same as (e) but with applied load. Above a threshold stress IKBs—comprised of coaxial dislocation loops that form on easy glide planes of KNE solids—form. The IKBs only extend to the ends of a grain where they are arrested by grain boundaries. Increasing the load results in their expansion. Removal of the load leads to their annihilation.

pressed Cd hexagonal single crystals with their basal planes almost parallel to the compression axis. He concluded that kink boundaries consist of planes which bisect the angle between the glide planes on either side of them and along which dislocations are concentrated.[46] A few years later, Hess and Barrett[47] proposed a model to explain kink band formation by the regular glide of dislocations. The major elements of their model are summarized schematically in Figs. 1(a)–1(d). Initially and upon loading, elastic bending [Fig. 1(a)] creates a maximum shear stress in the center of the column [Fig. 1(b)]. Above a critical value this shear stress is sufficient to create, within the volume that is to become the kink band, pairs of dislocations of opposite sign that move in opposite directions [Fig. 1(c)]. The end result is two regions of severe lattice curvature, separated from each other, and from the unkinked crystal, by well-defined kink boundaries, BC and DE [Fig. 1(d)]. These kink planes or boundaries have an excess of edge dislocations of one sign, which, in turn, is responsible for the lattice rotations observed. The combination of the two kink boundaries and the region between them defines a KB.

And while kink boundaries are irreversible, in order to explain many of our observations, including the ones reported herein, we had to invoke the idea of an incipient kink band or IKB, that by definition is fully reversible. IKBs are subcritical kink bands that at a threshold stress become critical. IKBs, however, only grow to the edges of the grains in which they nucleated [Fig. 1(f)]. The IKBs only exist as long as a load is applied. Removing the load results in their spontaneous collapse and a return to the virgin crystal [Fig. 1(e)]. It is important to stress here that the grain boundaries are what keeps the IKBs from devolving into regular irreversible kink bands [Fig. 1(d)]. It is also important to note that an IKB is comprised of parallel coaxial dislocation loops that nucleate on the basal or easy slip planes [Fig. 1(f) and inset in Fig. 2(a)]. In the next section we summarize Frank and Stroh's approach to the problem and our extension of it.

II. INCIPIENT KINK BANDS

Frank and Stroh, considered an elliptic KB with a length, 2α, and maximum width, 2β, such that $2\alpha > 2\beta$ [inset in Fig. 2(a)] and showed that the remote shear stress, τ, needed to render such a subcritical KB unstable—i.e., grow spontaneously—is given by[20]

$$\tau > \tau_c \approx \frac{\sigma_c}{M} \approx \sqrt{\frac{4G^2 b\gamma_c}{2\alpha\pi^2}\ln\left(\frac{b}{\gamma_c w}\right)}, \tag{1}$$

where τ_c and σ_c are the remote critical shear and axial stresses, respectively; G is the shear modulus, b is the Burgers vector, and w is related to the dislocation core width;[20] γ_c is the critical kinking angle. M is the Taylor factor that we introduced to relate the shear stress at the grain level to the uniaxial stress applied. Herein, M is assumed to be 3.

An IKB consists of multiple parallel dislocation loops [inset in Fig. 2(a)]. The formation of an IKB can be divided into two stages: nucleation and growth.[15] In our model, only IKB growth from $2\beta_{xc}$ and $2\beta_{yc}$ to $2\beta_x$ and $2\beta_y$, respectively, is considered. The values $2\beta_{xc}$ and $2\beta_{yc}$ represent the critical radii of the IKBs. It follows that for $\sigma > \sigma_t$, the IKB nuclei grow and the IKBs induced axial strain resulting from their growth is assumed to be given by[15]

$$\varepsilon_{\mathrm{IKB}} = \frac{4\pi(1-\nu)N_k\alpha^3}{3k_1G^2\gamma_c M^2}(\sigma^2 - \sigma_t^2) = m_1(\sigma^2 - \sigma_t^2), \tag{2}$$

where N_k is the number of IKBs per unit volume; ν is Poisson ratio; m_1 is the coefficient before the term in brackets in the second term. k_1 relates the volumetric shear strain to the macroscale uniaxial strain. k_1 varies from 1 to 2 and depends on texture.[16] Herein a value of 2 was adopted following the suggestion of Reed-Hill.[48]

The threshold stress, σ_t, is the remote axial stress needed to nucleate an IKB. If a sample is loaded to a stress $< \sigma_t$, IKBs do not form; no hysteresis is observed and the response is linear elastic. In many cases the threshold stress, σ_t, can be equated with σ_c, in which case, Eq. (1) can be rewritten as[15,16]

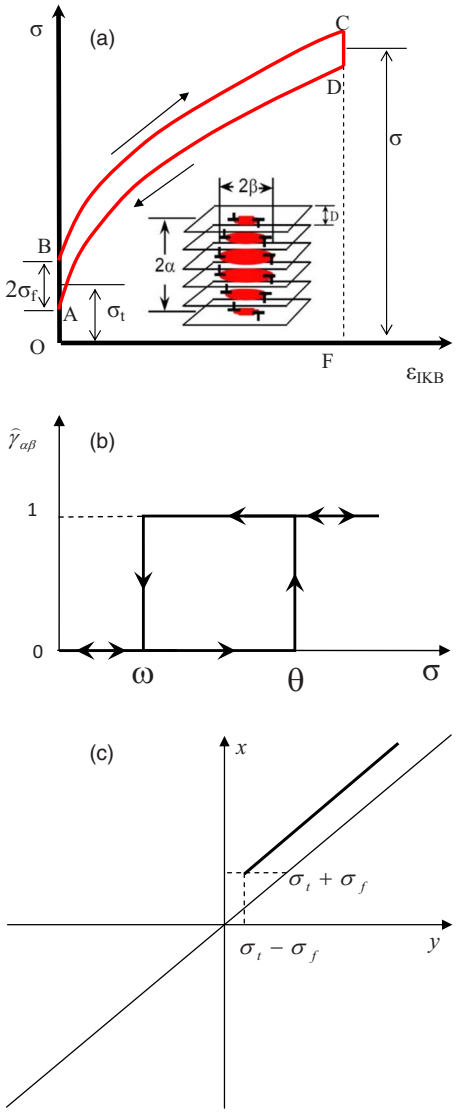

FIG. 2. (Color online) (a) Typical stress-strain curve of a single IKB. The inset is the schematic of an IKB. (b) Rectangular hysteretic loop of simple PM model. (c) An individual hysteretic element of a nonrectangular shape that corresponds to an IKB. x is the stress value during loading; y is the stress value during unloading. The distribution varies only along the two solid lines.

$$\sigma_t = \sigma_c = M\sqrt{\frac{4G^2 b\gamma_c}{2\alpha\pi^2}\ln\left(\frac{b}{\gamma_c w}\right)} = \left[M\sqrt{\frac{4G^2 b\gamma_c}{2\pi^2}\ln\left(\frac{b}{\gamma_c w}\right)}\right]\alpha^{-1/2} = C_1\alpha^{-1/2}, \tag{3}$$

where C_1 is the coefficient in the square brackets. Also in most cases, 2α is the grain dimension along the c axis of the hexagonal solids.[8,9,49] A notable exception is polycrystalline Co with grains larger than 80 μm, where 2α is $<$ the grain size.[17,50,51]

The energy dissipated per unit volume per cycle, W_d, viz. the area of a hysteretic loops—resulting from the growth and shrinkage of the IKBs from β_{ic} to β_i is given by[15]

$$W_d = \frac{4\pi(1-\nu)N_k\alpha^3}{G^2\gamma_c M^2}\frac{\Omega}{b}(\sigma^2-\sigma_t^2) = 3k_1\frac{\Omega}{b}m_1(\sigma^2-\sigma_t^2), \tag{4a}$$

which when combined with Eq. (2) yields

$$W_d = 3k_1\frac{\Omega}{b}\varepsilon_{\mathrm{IKB}}, \tag{4b}$$

where Ω is the energy dissipated by a dislocation line sweeping a unit area. Thus, Ω/b should be proportional, if not equal, to the critical resolved shear stress, CRSS, of an IKB dislocation loop. In previous work we have shown that to be the case.[8,9,15,16,49]

In deriving Eqs. (2) and (4) the following implicit simplifying assumptions were made: (i) all IKBs have the same average size and (ii), they are all oriented in the same average orientation with respect to the applied stress. The IKBs must be inclined with respect to the applied stress in order to nucleate. Said otherwise, M and k_1 are fixed and known. In real polycrystalline solid a distribution exists. One of the aims of this work is to try and shed some light on these distributions. To do so it is necessary to describe the response of a *single* IKB to stress.

During loading the true stress required to extend an IKB dislocation loop is $\sigma_a = \sigma - \sigma_f$, where σ_f is the friction force of the dislocation segments gliding on the basal planes. Note that in reality it is the shear stress that causes the loops to grow or shrink. That is why the M term was introduced in Eq. (2). Since σ_f and σ have opposite directions, if $\sigma_a > \sigma_t$, the IKB grows and Eq. (2) can be recast as

$$\varepsilon'_{\mathrm{IKB}} = m_{1,i}[(\sigma-\sigma_f)^2-\sigma_t^2], \tag{5}$$

where the average m_1 is replaced by an $m_{1,i}$ that depends on the orientation of a given IKB to the applied load, reflected in M_i in Eq. (2). During unloading, the same IKBs shrink. In this case, both σ and σ_f resist the shrinkage and $\sigma_a = \sigma + \sigma_f$. It follows that on the return path $\varepsilon_{\mathrm{IKB}}$ is given by

$$\varepsilon'_{\mathrm{IKB}} = m_{1,i}[(\sigma+\sigma_f)^2-\sigma_t^2]. \tag{6}$$

Based on Eqs. (5) and (6), the stress-strain response of a single IKB in a unit volume is shown in Fig. 2(a). Note that σ_t is defined midway between the loading and unloading paths. The width of the hysteretic loops, on the other hand, is $2\sigma_f$.

Referring to Fig. 2(a), the area encompassed within the hysteresis loop can be approximated as the difference in areas of the trapezoids OADF and OBCF. Noting that the strain of one IKB, $\varepsilon'_{\mathrm{IKB}} = \mathrm{OF}$, $\mathrm{CF} = \sigma + \sigma_f$, and $\mathrm{DF} = \sigma - \sigma_f$, it can be shown that for one IKB, $w_{d,1}$ is given by

$$w_{d,1} \approx 2\sigma_f\varepsilon'_{\mathrm{IKB}}. \tag{7}$$

If the sum of N_k IKBs strains is equated to the macroscopically measured, $\varepsilon_{\mathrm{IKB}}$, and $W_d = N_k w_{d,1}$, then by combining Eqs. (4b) and (7) it follows that

$$\sigma_f = \frac{3}{2} k_1 \frac{\Omega}{b}, \tag{8}$$

which, not too surprisingly, relates the friction force to the CRSS of the basal-plane dislocations.

It follows that if a relationship between IKBs and the PM model exists then the response of a polycrystal should result from the collective, but *independent*—a major tenet of the PM model—response of a distribution of IKBs. Note that the latter are confined to single grains and each is characterized by distinct values of σ_t and σ_f. It is also important to note that the variations in σ_f are *not* due to variations in Ω/b—which is identical to the CRSS of the dislocations making up the IKBs and is thus a material property—but rather to variations in the orientation of the basal planes relative to the direction of applied load, which is reflected in k_1. We note in passing that k_1 and M have to be related.

III. PM MODEL

Before discussing the important ramifications of this conclusion, the power of this model in predicting, or recreating, the strain after a complicated load history is demonstrated. In the following section we outline two analyses of the results: a simple PM model and a more sophisticated one, based on our IKB model.

(i) *Phenomenological PM model based on rectangular hysteretic units* [Fig. 2(b)]. In the mathematical PM model, the state of a material system is determined by the collection operators $\hat{\gamma}_{\theta\omega}$ with rectangular hysteresis loops [Fig. 2(b)]. The output strain ε of each $\hat{\gamma}_{\theta\omega}$ can only be 0 or 1. Every $\hat{\gamma}_{\theta\omega}$ has one up-threshold stress, θ, and one down-threshold stress, ω, such that $\theta > \omega > 0$. For loading from 0, $\hat{\gamma}_{\theta\omega}=0$ if $\sigma < \theta$. If $\sigma \geq \theta$ then $\hat{\gamma}_{\theta\omega}=1$. During unloading, because of friction, $\hat{\gamma}_{\theta\omega}=1$, if $\sigma > \omega$ and $\hat{\gamma}_{\theta\omega}=0$, if $\sigma \leq \omega$. This operation forms the rectangular loop illustrated in Fig. 2(b). If the contribution of operator $\hat{\gamma}_{\theta\omega}$ to the overall strain is $\mu(\theta,\omega)$ [function $\mu(\theta,\omega)$ is sometimes called PM or Preisach density], then the output of this transducer after a given load history is the sum of the outputs of all $\hat{\gamma}_{\theta\omega}$ weighted by $\mu(\theta,\omega)$ or[27]

$$\varepsilon(t) = \hat{\Gamma}\sigma(t) = \int \int_{\theta \geq \omega} \mu(\theta,\omega)\hat{\gamma}_{\theta\omega}\sigma(t)d\theta d\omega. \tag{9}$$

Note that at any σ there can be multiple values of strain—and vice versa. The time, t, is introduced here only to indicate that both the stress and strain are measured at the same moment in time, *not* that they are time dependent. Also note that $\mu(\theta,\omega)$ is not a probability density function of IKBs with various parameters. It is not even a probability density of operators $\hat{\gamma}_{\theta\omega}$ because it is not normalized. $\varepsilon(t)$ can be calculated by double integration if $\mu(\theta,\omega)$ is known. $\mu(\theta,\omega)$ can be obtained by double differentiation of the experimentally obtained first-order reversal curves such as those shown in Fig. 3(a). However, it is not necessary to actually differentiate experimental data and then carry out integration to obtain $\varepsilon(t)$. Instead, one can define an auxiliary function known as the Everett function related directly to differences

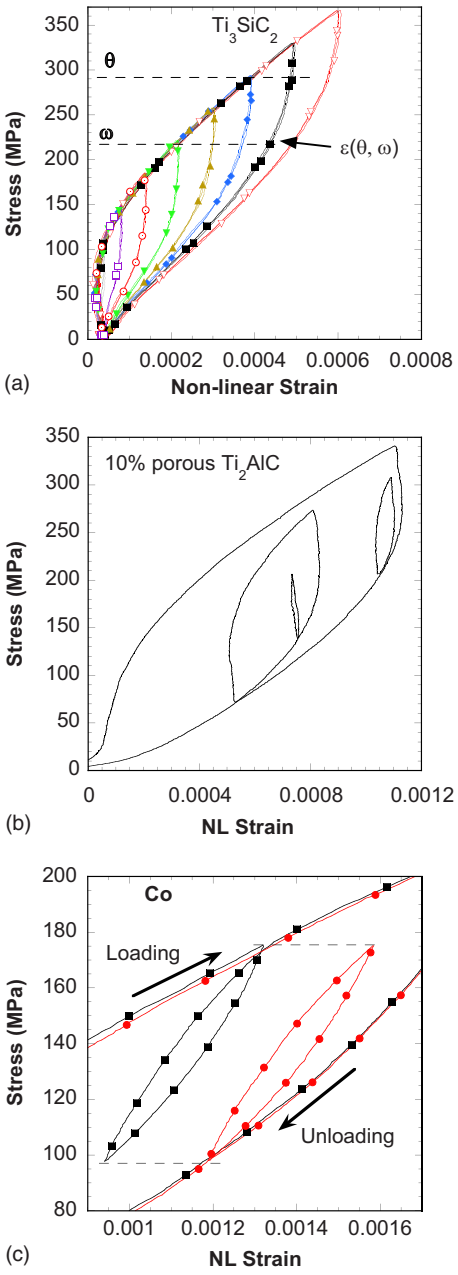

FIG. 3. (Color online) Stress-nonlinear strain curves of (a) Ti_3SiC_2, (b) porous Ti_2AlC, and (c) Co.

of $\varepsilon(t)$ obtained at $\sigma(t)$ along different reversal curves. All calculations of the output of the PM model can be carried out only on the basis of this Everett function.[26]

A simple calculation can be carried out if one follows the algorithm proposed in Refs. 26 and 29 which use parametric fitting involving just summation and subtraction of typical experimental results such as the nested loops shown in Fig. 3(a). This approximate method permits a relatively simple graphical construction of the Preisach space distribution function (PM density) and can be used for the simulation of any arbitrary stress-strain relationship.

It should be stressed that the PM model as described above is convenient for modeling of history-dependent stress-strain constitutive relationship. Its computational sim-

plicity (particularly when the computations are carried out using the Everett function) makes the model convenient in modeling systems constructed on the basis of solids described by the PM constitutive law. In some cases the rectangular loop operators may also have physical meaning. However, this is probably not the case for the KNE solids considered herein. Indeed, behavior of each IKB is clearly not described by the rectangular hysteresis loop associated with operator $\hat{\gamma}_{\theta\omega}$. The PM function $\mu(\theta,\omega)$ also does not have a clear physical meaning in this case.

The question may arise: could the PM model be recast in the form of superposition of independent IKBs? This might be useful for the purpose of identifying distributions of IKB parameters from experimental data and, thus, providing a more physically meaningful material characterization.

(ii) *IKB-based PM model based on the hysteretic unit shown in* Fig. 2(a). In order to recast the PM model in terms of distribution of independent IKBs, we start with the Everett function for a single isolated IKB [Fig. 2(a)] given by

$$\begin{aligned} E(x-\sigma_f, y+\sigma_f, \sigma_t) = {} & m_1 s(x-y-2\sigma_f) s[x-(\sigma_t+\sigma_f)] \\ & \times[(x-\sigma_f)^2-\sigma_t^2] - m_1 s(x-y-2\sigma_f) s \\ & \times[y-(\sigma_t-\sigma_f)][(y+\sigma_f)^2-\sigma_t^2], \end{aligned} \quad (10)$$

where x is the stress value during loading; y is the stress value during unloading; $s(x)$ is a unit step function (unity for positive arguments, zero for negative arguments). m_1, defined in Eq. (2), can be viewed as the amplitude of an IKB.

The Preisach distribution for such an isolated IKB is calculated through double differentiation of the Everett function[26]

$$\begin{aligned} & \frac{\partial E(x-\sigma_f, y+\sigma_f, \sigma_t)}{\partial x} \\ & = m_1 \delta(x-y-2\sigma_f) s(y+2\sigma_f-\sigma_t-\sigma_f) \\ & \quad \times[(y+2\sigma_f-\sigma_f)^2-\sigma_t^2] + m_1 s(\sigma_t+\sigma_f-y-2\sigma_f) \\ & \quad \times \delta(x-\sigma_t+\sigma_f)[(\sigma_t+\sigma_f-\sigma_f)^2-\sigma_t^2] + m_1 s \\ & \quad \times[x-(\sigma_t+\sigma_f)] s(x-y-2\sigma_f)(x-\sigma_f) \\ & \quad - m_1 \delta(x-y-2\sigma_f) s[y-(\sigma_t-\sigma_f)][(y+\sigma_f)^2-\sigma_t^2] \\ & = m_1 s[x-(\sigma_t+\sigma_f)] s(x-y-2\sigma_f)(x-\sigma_f), \end{aligned} \quad (11)$$

where δ is the Dirac's delta function. Taking into account the shifting property of the delta function, Eq. (11), can be simplified to

$$\begin{aligned} \mu(x,y,\sigma_t,\sigma_f) &= \frac{\partial^2 E(x-\sigma_f, y+\sigma_f, \sigma_t)}{\partial x\, \partial y} \\ &= -m_1 s(x-(\sigma_t+\sigma_f)) \delta(x-y-2\sigma_f)(x-\sigma_f). \end{aligned} \quad (12)$$

Graphically, the region of support of this distribution on the Preisach plane is shown in Fig. 2(c). Note that this region of support is a line parallel to the $x=y$ line in the Preisach plane. This suggests the following more convenient variables than x and y, viz.,

$$\Gamma = \frac{x+y}{2} \quad \text{and} \quad \eta = \frac{x-y}{2}. \quad (13)$$

Transforming Eq. (12) in terms of Γ and η gives

$$\begin{aligned} \tilde{\mu}(\Gamma,\eta,\sigma_t,\sigma_f) &= -m_1(\sigma_t) s[\Gamma+\eta-(\sigma_t+\sigma_f)] \\ &\quad \times \delta(2\theta-2\sigma_f)(\Gamma+\eta-\sigma_f) \\ &= -m_1(\sigma_t)\Gamma s(\Gamma-\sigma_t)\delta(\eta-\sigma_f). \end{aligned} \quad (14)$$

It follows that, the Preisach function of the entire system, which consists of many IKBs with different values of σ_t and σ_f, is given by

$$\begin{aligned} \varphi(\Gamma,\eta) &= \int_{-\infty}^{\infty}\int_{0}^{\infty} \rho(\sigma_t,\sigma_f)\tilde{\mu}(\Gamma,\eta,\sigma_t,\sigma_f) d\sigma_f d\sigma_t \\ &= -\int_{-\infty}^{\infty}\int_{0}^{\infty} \rho(\sigma_t,\sigma_f) m_1 \Gamma s(\Gamma-\sigma_t)\delta(\eta-\sigma_f) d\sigma_f d\sigma_t \\ &= -\int_{-\infty}^{\infty} m_1(\sigma_t)\Gamma s(\Gamma-\sigma_t) \\ &\quad \times \int_{0}^{\infty} \rho(\sigma_t,\sigma_f)\delta(\Gamma-\sigma_f) d\sigma_f d\sigma_t \\ &= -\Gamma\int_{-\infty}^{\infty} m_1(\sigma_t)\rho(\sigma_t,\eta) s(\Gamma-\sigma_t) d\sigma_t \\ &= -\Gamma\int_{-\infty}^{\Gamma} m_1(\sigma_t)\rho(\sigma_t,\eta) d\sigma_t, \end{aligned} \quad (15)$$

where $\rho(\sigma_t,\sigma_f)$ can be interpreted as the probability density of IKBs, each parametrized by different values of σ_t and σ_f. This probability density function can be computed from Eq. (15) since

$$\rho(\Gamma,\eta) = -\frac{1}{m_1}\frac{\partial}{\partial\Gamma}\left[\frac{1}{\Gamma}\varphi(\Gamma,\eta)\right] = -\frac{1}{m_1}\frac{\partial}{\partial\Gamma}\left[\frac{1}{\Gamma}\frac{\partial^2 E(\Gamma,\eta)}{\partial\Gamma\,\partial\,\eta}\right] \quad (16)$$

and m_1 is defined in Eq. (2). If $N_k=1$, then m_1 is only related with 2α, the length of this particular IKB. Combining Eqs. (2), (3), and (16) yields

$$\rho(\Gamma,\eta) = -\frac{3k_1 G^2 \gamma_c M^2}{4\pi(1-\nu)C_1^6}\cdot\sigma_t^6\cdot\frac{\partial}{\partial\Gamma}\left(\frac{1}{\Gamma}\frac{\partial^2 E(\Gamma,\eta)}{\partial\Gamma\,\partial\,\eta}\right). \quad (17)$$

Thus, recasting the PM model, which has been shown here to completely describe KNE solids, in terms of independent IKBs permits one to characterize the material in terms of the probability density of the IKBs.

IV. EXPERIMENTAL DETAILS

Herein three representative KNE solids were examined. They were cobalt (99.97%, ESPI metals, Ashland, OR) (Ref. 15) annealed at 1000 °C for 4 h; Ti_3SiC_2 fabricated by hot pressing[8] at 1600 °C for 4 h, and a 10 vol % porous Ti_2AlC made by pressureless sintering[9] at 1500 °C for 1 h in flowing Ar.

The processing, microstructural and testing details can be found elsewhere.[8,9,15] Briefly, cylinders (diameter =9.7 mm, length=31 mm) were electrodischarge machined and cyclically compressed, to different stress levels using a hydraulic testing machine (MTS 810, Minneapolis, MN), supplied with a controller (Microconsoler 458.20, MTS). An extensometer (MTS 632.59C-01) with a 25 mm gauge length attached directly to the sample was used to measure the strains.

V. RESULTS AND DISCUSSION

As in our previous work,[8] when the Ti_3SiC_2 sample was loaded to progressively higher loads, reproducible, closed, time invariant, hysteresis loops [Fig. 3(a)] were obtained. In this figure, the linear elastic strain, assuming a Young's modulus of 325 GPa, was removed from the total strain. Similar loops were obtained for Co (Ref. 15) and Ti_2AlC.[9] Note the unique loading, but multiple unloading trajectories. The latter depends on the maximum stress from which the unloading occurs.

Figure 3(a) clearly illustrates the wiping-out property of Ti_3SiC_2. When a sample is loaded to a stress σ, all minor (intermediate) loops obtained below that stress are wiped out; i.e., there is complete loss of memory or load history. The same is true for the 10 vol % porous Ti_2AlC sample [Fig. 3(b)]; during unloading, all minor loops are closed and are wiped out by a larger unload.

Congruency is illustrated in Fig. 3(c). Here the minor loops for Co, obtained when the stress is cycled between 100 and 170 MPa, are congruent and independent of whether the loops were obtained on loading *or* unloading. Similar results[52] were obtained for all solids examined herein. Clearly, the results shown in Fig. 3 satisfy the two criteria needed for a hysteresis to be adequately described by the PM model.

The PM density function for Ti_3SiC_2 is plotted in Fig. 4(a), where the highest densities correspond to the darkest areas. Note that the linear elastic component to the strain was subtracted out prior to determining the PM density function. Including it does not change the shape of the space, but because the elastic component is so much higher than the nonlinear elastic component, it tends to overshadow the latter. For the sake of illustration, we schematically show, as insets in Fig. 4(a), the relative shape of the various elements represented by the various regions on the map. Similar maps were obtained for polycrystalline Co [Fig. 4(b)] and the 10 vol % porous Ti_2AlC [Fig. 4(c)]. In all cases, the highest densities roughly fall on a 45° line.

And while the rectangular hysteretic units [Fig. 2(b)] are phenomenological, nevertheless once the PM space is determined, this model is very powerful in predicting the response of KNE solids to complicated stress/strain trajectories. The aforementioned approach was applied to reconstruct the strains of the porous Ti_2AlC [Fig. 5(a)] and Co [Fig. 5(b)] samples loaded to arbitrary intermediate stress levels. The agreement between the measured and predicted strains is excellent in both cases, further solidifying our important claim that KNE solids can be described by the PM model. It follows that for a KNE solid, once a set of $\mu(\theta,\omega)$ is experimentally determined, the strain of this solid, for *any* deformation history, can be predicted or modeled by the PM distribution (Fig. 4). In other words, once the distribution of the hysteretic elements are known, one can determine all macroscopic stress-strain relations.

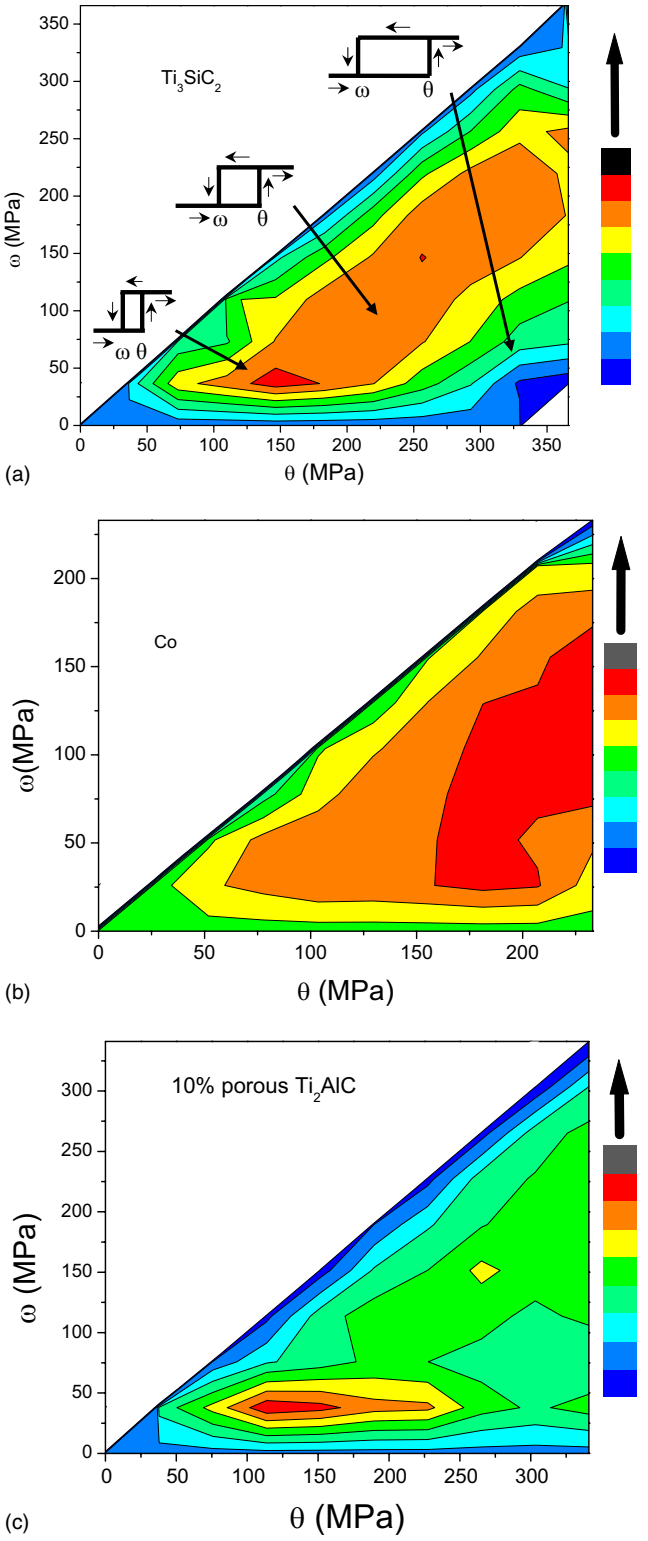

FIG. 4. (Color online) PM density of (a) Ti_3SiC_2, (b) Co, and (c) porous Ti_2AlC.

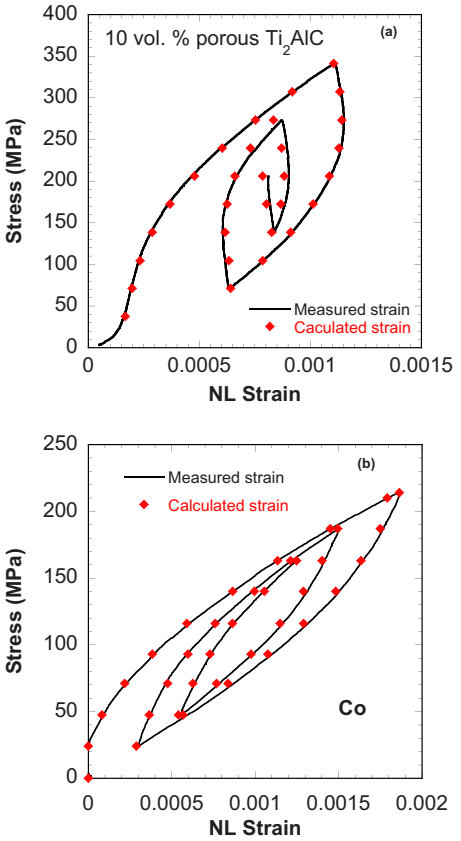

FIG. 5. (Color online) Calculated and experimental stress-nonlinear-strain curves of (a) porous Ti_2AlC (b) Co.

Figure 6(a) shows the distribution of IKBs—assuming the individual hysteretic elements behave as shown in Fig. 2(a)—for polycrystalline Co. The distributions for Ti_3SiC_2 and 10 vol % porous Ti_2AlC samples are plotted in Figs. 6(b) and 6(c), respectively.[52] In all cases, the probability of IKBs with relatively high σ_t's is high. This implies that in all cases, the grain size, or 2α, is either small or poorly oriented vis-à-vis the loading direction. Interestingly, since, (i) it is true that the number of fine grains is much larger than that of coarse grains in any polycrystalline sample but; (ii) some coarse grains with low σ_t's can induce large nonlinear strains [according to Eq. (17), ρ is proportional to σ_t^6!], it follows that the number distribution of IKBs does not give us much information about the physics of the IKBs because it is highly skewed to the fine grains.

This comment notwithstanding, these distributions, can be used to determine the distributions of σ_t and σ_f, achieved by summing the columns or rows of the distribution matrix. The results are shown in Figs. 7(a) and 7(b) for σ_t and σ_f, respectively.

Threshold and friction stresses

Because σ_t is related to grain size [Eq. (3)], the distribution of σ_t's should reflect the distribution of grain sizes. As shown in Fig. 7(a), clearly, the distribution has a maximum value at some intermediate stress value. The narrowness or width of the distribution should reflect a sample's texture.

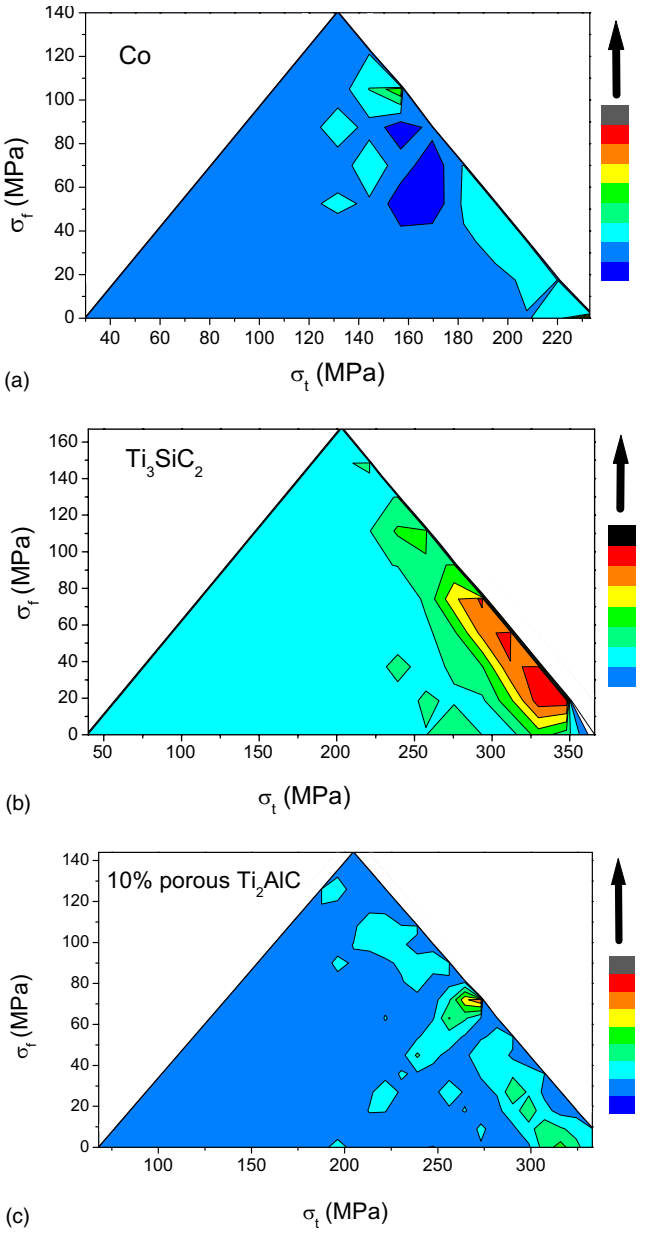

FIG. 6. (Color online) IKB distribution of (a) Co, (b) Ti_3SiC_2, and (c) porous Ti_2AlC.

Correlating the latter with the results shown in Fig. 7(a), while beyond the scope of this paper—is a worthwhile exercise that we are currently addressing. As noted above, since this is a number distribution it, per force, more strongly reflects the fine grains' influence on the hysteresis. This is true despite the fact that the coarse grains, despite their smaller number, play a more important hysteretic role.

According to Eq. (8), if $k_1=2$, σ_f is three times the CRSS. Figure 7(b) shows the distributions in σ_f's together with the values of three times the CRSS obtained from our simple analytical model.[9,17] Here again, it is reasonable to assume that the differences between the various distributions and the respective CRSS reflect differences in grain sizes and textures.

The conclusion that KNE solids, in their ubiquity, can be described by the PM model has several important implica-

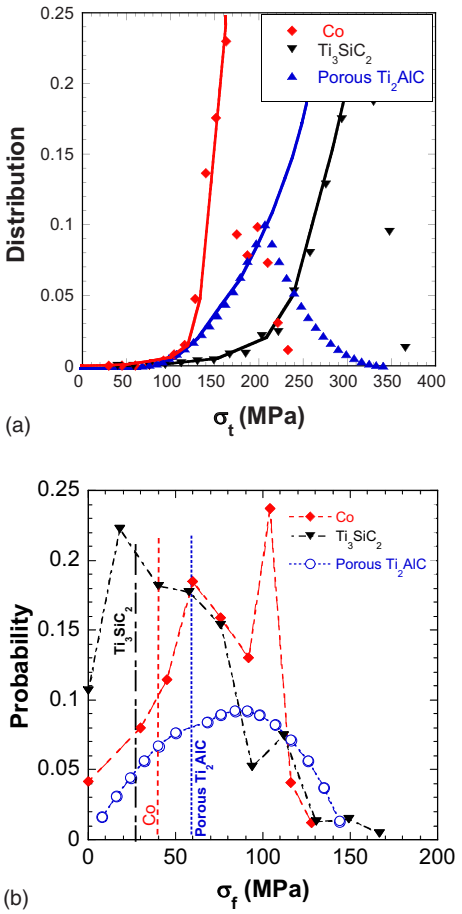

FIG. 7. (Color online) (a) Distributions of σ_t, (b) distributions of σ_f together with the values of CRSS. The vertical dashed lines represent the σ_f values that correspond to three times the CRSS determined using our analytic IKB model for the same samples. In all cases k_1 was assumed to be 2. The agreement is excellent given the simplifying assumptions made.

tions. First, one of the fundamental underlying assumptions of the PM model is that the behavior of the individual independent hysteretic units—IKBs in our case—is transferred to the behavior of the whole sample. It follows that despite the fact that many IKBs are expected to interact in various ways, one can conclude that they still behave as a collection of *independent* hysteretic units of the same type. Note this does not mean that the IKBs do not interact, instead it implies that whatever interactions, if any, occur do not qualitatively change the behavior or shape of the underlying hysteretic units. Said otherwise, despite possible, but unlikely, interactions, each individual unit continues to display wiping out and congruency which the entire system, therefore, inherits; a truly remarkable result.

The fact that key properties of the individual IKBs are preserved in bulk polycrystalline KNE solids has several important practical implications. First, as we show, the constitutive equations are known and can be used to accurately predict the response of KNE solids to complicated stress histories. That this model can be used to describe the behavior of the over 60 MAX phases known, Co, Mg, Zr, and possibly their alloys—all technologically important solids—among many others is significant. At this junction it is important to point out that the PM model can only be used when the system is in a pure IKB regime. In some solids, at higher temperatures and/or stresses, the IKBs can be sundered and transform to mobile dislocation walls that, in turn, result in permanent deformation and creep. In those situations, the system can no longer be adequately described by the PM model since the response has an inelastic component.[7,53] However, since in most cases, cycling to the same stress a few times, rids the system of non-IKB-related dislocations,[9,15] the PM model would still be applicable as long as the maximum stress does not exceed the highest stress level experienced by the sample.

Second, the need to prove congruency and end-point memory for at least some KNE solids, again in all their ubiquity, is no longer needed simplifying future experiments. This comment notwithstanding, it is hereby acknowledged that, we are just starting to understand KNE solids and it is possible, that further work shows a subcategory of KNE solids that may not exhibit congruency. We also acknowledge that while obtaining the distribution of hysteretic elements (Figs. 4 and 6) is straightforward, it is time consuming.

Third, we recently proposed to use KNE solids as stress/strain sensors where the stress history of the sample can be continually monitored.[54] Having a robust constitutive model for how these solids respond to stress is an important and necessary condition for implementation of this idea. The fact that, in some cases, the response is a weak function of temperature—at least for Ti_3SiC_2 (Ref. 7)—bodes well for the use of these solids as high-temperature sensors.

Along those lines it is important to note that for all materials tested there is a consistency in the form of the Preisach distribution function. Specifically, to a good approximation the curves of the Preisach function, over the plane of the upper and lower switching thresholds are nearly parallel to the $\theta=\omega$ line [Fig. 4(a)]. This implies that the Preisach distribution is mostly a function of the difference $\theta-\omega$, rather than on θ and ω separately, which, in turn, has important implications. Specifically, when the Preisach function depends only on $(\theta-\omega)$, it can be shown that the inverse hysteresis operator—where σ is treated as the output and strain as the input—is also of the Preisach type. This is particularly convenient in some potential applications, such as sensing or actuation, where both forward and inverse constitutive laws need to be computed quickly. This form of the Preisach function also demonstrates that parametrization of the model may be reduced ($\theta-\omega$ is a single parameter instead of two separate θ and ω parameters) suggesting that the irreversible behavior is dominated by frictional IKB growth and shrinkage processes, rather than their appearance and disappearance in agreement with our microscale modeling.[15] These comments notwithstanding, this hypothesis requires additional testing that we hope to perform in the near future.

Fourth, the results shown in Fig. 5 are invaluable to any modeling, especially finite element, of the deformation of the KNE solids. Our results can be used to either guide the modeling efforts or act as a check on their validity.

Fifth, based on our understanding of KNE solids they should not experience measurable fatigue. In fact, their behavior stabilizes in response to a cyclic load after a few

cycles. This suggests that such materials are ideally suited for a situation where cyclic loading can affect the longevity of engineering structures. Indeed preliminary results on Ti_3SiC_2,[7] and other KNE solids such as C-plane sapphire,[18] have been shown to produce the identical hysteretic stress-strain curves even when cycled to relatively high stresses. For example, we showed that sapphire single crystals can be repeatedly loaded, up to 30 times, with a spherical indenter to stresses greater than 30 GPa without evidence of creep or fatigue.[18] This distinction is important in differentiating between hysteresis that is not truly time or cycling invariant, such as microcracking, for example, and what we are proposing here, where the cycles are truly repeatable and reproducible.

In summary, because the nonlinear hysteretic response of KNE solids exhibits wiping out and congruency, the PM model is applicable. Once the distribution of independent hysteretic elements is determined, the model can be used to predict the response of these materials to complex stress histories remarkably well. Lastly we note that the conclusions of this work are valid *regardless* of the exact nature of the microscopic hysteretic units. Consequently, if further work, however unlikely, shows that the hysteretic units are *not* IKBs, but rather another micromechanism, the conclusions of this work do *not* change: KNE solids can be rigorously described by the PM model.

ACKNOWLEDGMENTS

This work was supported by the Army Research Office (Grant No. W911NF-07-1-0628).

*Present address: School of Materials Science and Engineering, Henan Polytechnic University, Jiaozuo, Henan 454100, China.
†Present address: Naval Undersea Warfare Center, Newport, RI 02841.
‡On leave from NRCN, Israel.

[1] J. B. Walsh, J. Geophys. Res. **71**, 2591 (1966).
[2] B. R. Lawn and D. B. Marshall, J. Mech. Phys. Solids **46**, 85 (1998).
[3] V. Aleshin and K. Van Den Abeele, J. Mech. Phys. Solids **55**, 765 (2007).
[4] J. B. Walsh, J. Geophys. Res. **70**, 399 (1965).
[5] X. Q. Feng and S. W. Yu, Theor. Appl. Fract. Mech. **34**, 225 (2000).
[6] M. Kachanov, W. H. John, and Y. W. Theodore, in *Advances in Applied Mechanics* (Elsevier, New York, 1993), Vol. 30, p. 259.
[7] M. W. Barsoum, T. Zhen, S. R. Kalidindi, M. Radovic, and A. Murugaiah, Nature Mater. **2**, 107 (2003).
[8] M. W. Barsoum, T. Zhen, A. Zhou, S. Basu, and S. R. Kalidindi, Phys. Rev. B **71**, 134101 (2005).
[9] A. G. Zhou, M. W. Barsoum, S. Basu, S. R. Kalidindi, and T. El-Raghy, Acta Mater. **54**, 1631 (2006).
[10] T. Zhen, M. W. Barsoum, and S. R. Kalidindi, Acta Mater. **53**, 4163 (2005).
[11] M. W. Barsoum, A. Murugaiah, S. R. Kalidindi, and T. Zhen, Phys. Rev. Lett. **92**, 255508 (2004).
[12] M. W. Barsoum, M. Radovic, T. Zhen, P. Finkel, and S. R. Kalidindi, Phys. Rev. Lett. **94**, 085501 (2005).
[13] A. G. Zhou and M. W. Barsoum, J. Alloys Compd. **498**, 62 (2010).
[14] M. W. Barsoum, A. Murugaiah, S. R. Kalidindi, T. Zhen, and Y. Gogotsi, Carbon **42**, 1435 (2004).
[15] A. G. Zhou, S. Basu, and M. W. Barsoum, Acta Mater. **56**, 60 (2008).
[16] A. Zhou and M. Barsoum, Metall. Mater. Trans. A **40**, 1741 (2009).
[17] A. G. Zhou, D. Brown, S. Vogel, O. Yeheskel and M. W. Barsoum, Mater. Sci. Eng., A **527**, 4664 (2010).
[18] S. Basu, M. W. Barsoum, and S. R. Kalidindi, J. Appl. Phys. **99**, 063501 (2006).
[19] S. Basu, A. G. Zhou, and M. W. Barsoum, J. Mater. Res. **23**, 1334 (2008).
[20] F. C. Frank and A. N. Stroh, Proc. Phys. Soc. London, Sect. B **65**, 811 (1952).
[21] R. A. Guyer, K. R. McCall, G. N. Boitnott, L. B. Hilbert, Jr., and T. J. Plona, J. Geophys. Res. **102**, 5281 (1997).
[22] K. R. McCall and R. A. Guyer, J. Geophys. Res. **99**, 23887 (1994).
[23] R. A. Guyer and P. A. Johnson, Phys. Today **52** (4), 30 (1999).
[24] *Systems with Hysteresis*, edited by M. Krasnoselskii and A. Prokrovskii (Nauka, Moscow, 1983).
[25] F. Preisach, Z. Phys. **94**, 277 (1935).
[26] *Mathematical Models of Hysteresis and their Applications*, edited by I. Mayergoyz (Elsevier, New York, 2003).
[27] I. D. Mayergoyz, Phys. Rev. Lett. **56**, 1518 (1986).
[28] R. A. Guyer, K. R. McCall, and G. N. Boitnott, Phys. Rev. Lett. **74**, 3491 (1995).
[29] J. Ortín, J. Appl. Phys. **71**, 1454 (1992).
[30] O. Mügge, Miner. **1**, 71 (1898).
[31] N. C. Gay and L. E. Weiss, Tectonophysics **21**, 287 (1974).
[32] R. E. Robertson, J. Polym. Sci., Part A-2 **7**, 1315 (1969).
[33] G. E. Attenburrow and D. C. Bassett, J. Mater. Sci. **14**, 2679 (1979).
[34] S. J. Deteresa, R. S. Porter, and R. J. Farris, J. Mater. Sci. **23**, 1886 (1988).
[35] D. A. Zaukelies, J. Appl. Phys. **33**, 2797 (1962).
[36] A. Keller and J. G. Rider, J. Mater. Sci. **1**, 389 (1966).
[37] C. T. Keith and W. A. Cote Jr., Forest Prod. J. **18**, 67 (1968).
[38] H. M. Hawthorne and E. Teghtsoonian, J. Mater. Sci. **10**, 41 (1975).
[39] W. R. Jones and J. W. Johnson, Carbon **9**, 645 (1971).
[40] V. Gupta, K. Anand, and M. Kryska, Acta Metall. Mater. **42**, 781 (1994).
[41] C. W. Weaver and J. G. Williams, J. Mater. Sci. **10**, 1323 (1975).
[42] A. S. Argon, in *Treatise on Materials Science & Technology*, edited by H. Herman (Academic Press, New York, 1972), Vol. 1, p. 79.
[43] M. S. Paterson, Geol. Soc. Am. Bull. **77**, 343 (1966).
[44] R. Christoffersen and A. K. Kronenberg, J. Struct. Geol. **15**,

1077 (1993).
[45] A. Kronenberg, S. Kirby, and J. Pinkston, J. Geophys. Res. **95**, 19257 (1990).
[46] E. Orowan, Nature (London) **149**, 643 (1942).
[47] J. B. Hess and C. S. Barrett, Trans. Am. Inst. Min. Eng. **185**, 599 (1949).
[48] R. E. Reed-Hill, E. P. Dahlberg, and J. W. A. Slippy, Trans. Am. Inst. Min. Eng. **233**, 1766 (1965).
[49] M. Fraczkiewicz, A. G. Zhou, and M. W. Barsoum, Acta Mater. **54**, 5261 (2006).
[50] H. -M. Thieringer, Z. Metallkd. **59**, 476 (1968).
[51] C. Hitzenberger, H. P. Karnthaler, and A. Korner, Acta Metall. **33**, 1293 (1985).
[52] A. G. Zhou, Ph.D. thesis, Drexel University, 2008.
[53] T. Zhen, M. W. Barsoum, S. R. Kalidindi, M. Radovic, Z. M. Sun, and T. El-Raghy, Acta Mater. **53**, 4963 (2005).
[54] P. Finkel, M. W. Barsoum, S. Basu, and A. G. Zhou, U.S. Patent Provisional application No. US 60/941865 00 (filed on 4 June 2007, pending).